Chromospheric line blanketing and the hydrogen spectrum in M dwarfs

C.I. Short and J.G. Doyle

Armagh Observatory, College Hill, Armagh BT61 9DG, Northern Ireland (cis@star.arm.ac.uk – jgd@star.arm.ac.uk)

Abstract. We present non-LTE calculations of the H I spectrum in a grid of chromospheric models that represents a dM0 star in which the activity level ranges from quiescent to very active. We investigate three different treatments of the background opacity: 1) continuous opacity only, 2) blanketing due to lines that form in the photosphere below T_{min}, and 3) blanketing by lines that form throughout the entire outer atmosphere. We show that the predicted W_λ of Lyα in all models is reduced by as much as a factor of ≈ 4, and that of Hα in very active (dMe) stars is enhanced by a factor of about two by the inclusion of background line opacity. A consistent treatment of line blanketing that includes the effect of the chromospheric and transition region temperature structure in the calculation of background line opacity is necessary for the accurate calculation of Lyα, and in some cases Hα, in these stars. The Hα line in less active models, and the Paβ line in all models, is negligibly affected by the treatment of background opacity. We also show that, in addition to the expected suppression of emergent flux in the visible by line blanketing, the broad-band continuum flux in regions where $\lambda < 2000 A$ is *increased* by as much as a factor of three in some models by the inclusion of line blanketing. This reduces the equivalent width of the Lyman series by a factor of four and is due to the veil of background lines going into emission in the UV, and to the stronger coupling of the background source function to the Planck function in the presence of blanketing by thermal lines. We confirm the results of earlier calculations that suggest the dominance of the *continuum* emission in the radiative cooling of the chromosphere. Therefore, any proposed heating mechanisms must supply at least an order of magnitude more non-radiative heating than would be required on the basis of an analysis in which only emission line cooling is considered. We also include a preliminary assessment of non-LTE effects in the background opacity on the emergent UV continua.

Key words: stars: late-type – stars: activity – stars: chromospheres – line: formation

1. Introduction

Strong spectral lines play a special role in the modelling of late-type stellar atmospheres because their cores are sensitive to the outer layers where poorly understood non-radiative heating processes affect the atmospheric structure (for a review, see Avrett 1990). The spectrum of H I plays a particularly important role, not only because it contains strong lines, but because the ionization balance of H I/H II in the outer atmosphere partly determines the atmospheric structure. In a recent series of papers, Doyle *et al.* (1994), Houdebine & Doyle (1994), Houdebine *et al.* (1995), and Houdebine *et al.* (1996) have explored the detailed line formation physics of the hydrogen spectrum in an extensive grid of chromospheric models of early M dwarfs. This monumental study includes an investigation of the response of the H I spectrum to atmospheric parameters and details of the chromospheric structure in models that span the entire range of observed activity level. This study provides a valuable guide to using H I lines as semi-empirical chromospheric diagnostics.

Among the modelling achievements and important results of the above study are the following: 1) the construction of low activity models that can reproduce the very weak Hα absorption of the "zero Hα" dM(e) stars and simultaneously reproduce the observed low surface flux of the Ca II HK and Mg II hk emission lines in these stars (Doyle *et al.* 1994); 2) the determination of constraints on the mass loading, (m_o), at the onset of the transition region at the top of the chromosphere (equivalent to determining the chromospheric pressure and the steepness of the chromospheric gradient or the thickness of the chromosphere for a given value of T_{min}), the temperature at the onset of the transition region (8500 K in most cases), and the thickness and functional form of the transition region that is required to simultaneously fit the self-reversed Hα and Hβ emission line profiles and the ratio of Lyα to Hα surface flux in the most active (dMe) stars (Houdebine & Doyle 1994); 3) the construction of a comprehensive grid of chromospheric models that successfully reproduces the observed morphology of the Hα line in dM stars, from the lowest activity dM(e) stars to intermediate activity stars with either strong Hα absorption or Hα emission wings and an absorption core, to the highest activity dMe stars with strong Hα emission. This grid has been used

to derive chromospheric diagnostics by comparing the relative response of the various series of the H I spectrum (Lyman to Brackett) to changes in the structure of both the lower and upper chromosphere (Houdebine *et al.* 1995); and, 4) the modelling of the H emission *continua* and the hitherto unexpected realization that these continua, rather than the emission line spectrum, is the dominant coolant in the chromospheres of those stars with relatively hot T_{min} values, and that the excess H I continuum emission in the highest activity stars decreases the $U - B$ colour to an extent that is observable (Houdebine *et al.* 1996).

In the present investigation, we refine the above study by including additional physics: line blanketing of the radiation field in the non-LTE treatment of hydrogen. In general, the cores of strong lines that form at relatively low gas densities high in the atmosphere differ greatly from those predicted by calculations done with the approximation of Local Thermodynamic Equilibrium (LTE) (see the review by Avrett 1990). As a result, the line under investigation may depend on radiative rates in other transitions of the atom, and these rates may be sensitive to the non-local radiation field. Therefore, a detailed description of the background radiation field may be important for an accurate solution of the non-LTE problem (see, for example, Mihalas (1978)). The reduction of non-LTE over-ionization in the UV continua of Fe I in the Sun due to the inclusion of line veiling in the background radiation field is a particularly instructive example (Rutten 1988).

Many previous non-LTE calculations of chromospheric lines have ignored line blanketing in the background radiation field. Some have included photospheric line opacity only, as in the case of the H I and Na I study in chromospheric dM star models by Andretta *et al.* (1997) (ADB henceforth), or the non-LTE multi-line chromospheric modelling of g Her (M6 III) by Luttermoser *et al.* (1994). Because the Lyman and Balmer line series and the Lyman continuum form well above T_{min}, the statistical equilibrium of hydrogen may be affected by blanketing due to lines that form in the chromosphere (and transition region in the case of Lyα) as well as blanketing due to photospheric lines. Therefore, we have used the recently developed PHOENIX model atmosphere code of Allard & Hauschildt (1995) to include line blanketing of the background radiation field throughout the entire outer atmosphere, taking into account the chromospheric and transition region temperature structure. We discuss the behavior of chromospheric and transition region line blanketing and assess its impact on the hydrogen equilibrium and line formation physics in chromospheric models.

2. Computational method

2.1. Atmospheric models

Because the calculation of moderate resolution line opacity over a range of 50 000 A is computationally intensive, we consider a restricted sample of six chromospheric models taken from the grid presented by ADB. These models have as their photospheric base a radiative equilibrium model calculated with PHOENIX (Allard & Hauschildt 1995). This photospheric model corre-
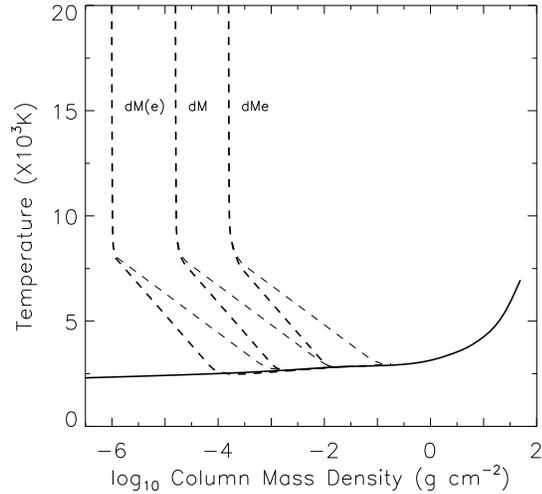
Fig. 1. Temperature structure of models in grid. $1A$ series: thin dashed line, $2A$ series: thick dashed line.

Table 1. Parameters of grid models

	Series $1A$		Series $2A$	
$\log m_{\mathrm{o}}$	T_{min}	$\log m_{\mathrm{min}}$	T_{min}	$\log m_{\mathrm{min}}$
-6.0	2660	-2.72	2480	-3.72
-4.8	2830	-1.70	2650	-2.70
-3.8	2960	-0.80	2810	-1.80

sponds to a star of T_{eff} = 3700 K, log g = 4.7, $[\frac{A}{H}]$ = 0.0, and ξ_{T} = 1.0 km s^{-1}. These parameters correspond to a star of spectral type dM0 or dM1 (Lang 1992; Mihalas & Binney 1981). The PHOENIX model atmosphere code includes many important diatomic and triatomic molecules such as TiO and H$_2$O in the equation of state and opacity data and has been shown to provide realistic models of *early* M stars (Allard & Hauschildt 1995).

From each of the two model series of ADB labeled $1A$ and $2A$, we take models with the smallest, largest, and an intermediate value of m_{o}, which is the mass loading at the onset of the transition region. These two model series differ in the value of $\frac{dT}{d\log m}$ in the chromosphere, with the series $2A$ models having a steeper chromospheric temperature rise. Therefore, comparison of spectral diagnostics computed with these two model series allows an assessment of the sensitivity to the location of T_{min} and the steepness of the chromospheric gradient (or, equivalently, the thickness of the chromosphere). The constancy of the chromospheric $\frac{dT}{d\log m}$ in these models is in keeping with the results of previous semi-empirical modeling of the outer atmospheres of a large variety of late-type stars (cf. Eriksson et al. 1983; Basri et al. 1981; Kelch et al. 1979 and other papers in those series). The value of $\frac{dT}{d\log m}$ in the transition region, $(\frac{dT}{d\log m})_{\mathrm{TR}}$, is also constant in these models, and we have chosen to use the sub-set of the grid that has a value of -6.5. The temperature at the top of the chromosphere where the transition region begins, $T(m_{\mathrm{o}})$, is

fixed at 8500 K following Houdebine & Doyle (1994). We only consider models that are in radiative equilibrium below T_{min}. Therefore, by fixing the value of T_{min}, we also fix the value of m_{min}, which is the mass loading at T_{min}. Table 1 shows the chromospheric parameters of the grid models, and Fig. 1 shows their temperature structure.

The increase in temperature throughout the chromosphere has an associated increase in the micro-turbulent velocity, ξ_T. In these models, ξ_T rises exponentially with decreasing log(m) in the chromosphere to a value of ≈ 10 km s^{-1} at m_O, then rises rapidly in the transition region to a value of ≈ 50 km s^{-1}. A value of 10 km s^{-1} at the top of the chromosphere is typical of values found for other late-type stars (see, for example, Eriksson et al. (1983) and papers in that series).

2.2. Line opacity

We have used PHOENIX to compute for our grid of models the mean of the total mass absorption due to lines, κ_l, in $2A$ intervals from 500 to $25000A$, and in $50A$ intervals from 25000 to $50000A$. The line lists used for the calculation incorporate those of Kurucz (1990), which contain about 58 million lines due to atoms and diatomic molecules, as well as the most recent and comprehensive line lists for molecules of particular importance in M stars such as TiO and H_2O. The total line list contains ≈ 70 million lines. The PHOENIX code was originally developed to compute atmospheric models of nova and supernova, therefore, it been proven over a wider range of temperature and density than most codes that are optimized for the atmospheric modelling of M stars. Furthermore, PHOENIX calculates the line opacity by direct Opacity Sampling rather than by pre-tabulated Opacity Distribution Functions. Therefore, we were able to compute κ_l at all depths from the base of the photosphere to a point in the lower transition region around a temperature of 20 000 K.

The temperatures and densities in the upper chromosphere and lower transition region in our models correspond to the partial ionization of H I, which is, therefore, the main e^- donor at those heights. The calculation of the ionization equilibrium of H I in the chromosphere is complicated by severe non-LTE effects. Therefore, the N_e structure used in the calculation of κ_l is calculated from a multi-level non-LTE solution of the coupled radiative transfer and statistical equilibrium equations for the first five levels of H I using an operator splitting/accelerated lambda iteration procedure that is incorporated into PHOENIX. The N_e structure and the value of κ_l in the chromosphere may also be affected by the non-LTE ionization of various metals. Therefore, we have also treated in non-LTE some of those species for which PHOENIX incorporates detailed atomic models: the first five levels of Mg II and Ca II, the first ten levels of He I and He II, and the first three levels of Na I.

2.3. Non-LTE hydrogen

We have used the code MULTI (Carlsson 1986) to solve the combined radiative transfer and statistical equilibrium equations

for an atomic model that incorporates the lowest nine levels of H I and the H II state. Because the chromospheric N_e density structure is determined by the H I/H II ionization balance, we iterate the non-LTE solution and the equation of hydrostatic equilibrium to convergence. The radiative transfer problem is solved in detail for all 36 $b - b$ transitions connecting the nine H I states and for the $b - f$ transitions of these states. The calculation of the background radiation field includes the addition of the PHOENIX line opacities, κ_l, to the continuous opacity normally computed by MULTI. These were incorporated using a modified version of MULTI that was presented in ADB. For the $b - b$ transitions, κ_l was included in the Lyα, Hα, and Paβ lines as a straight arithmetic mean in $2A$ intervals. We included blanketing in the first two of these because of their important role in the statistical equilibrium of H I, and in the latter because we wish to develop the detailed line shape of Paβ as a chromospheric diagnostic (Paα is generally too contaminated by telluric absorption to be a useful). For the $b - f$ transitions, κ_l was included as a harmonic mean in $100A$ intervals. An interval width of $100A$ is necessary because normally a sparse frequency sampling of the $b - f$ continua is used in MULTI calculations in order to control the computation time. A harmonic mean was used because occasional strong lines have a disproportionately large effect on the straight mean in a large wavelength interval.

ADB also included background line opacities computed with PHOENIX in their non-LTE H I/II calculation with the same models. However, they were able to compute κ_l for a photospheric model only. For their chromospheric models they gradually ramped the value of κ_l down to zero, *ad hoc*, over a decade in column mass density above T_{min}. In order to compare our results with previous studies, we have used our procedure to calculate κ_l for a radiative equilibrium model and ramped it down to zero just above T_{min} using the same procedure as ADB. We then re-calculated the non-LTE H I/II and N_e solution using these photospheric κ_l tables. For clarity, we henceforth designate as κ_l^c the line opacity that reflects the chromospheric and transition region temperature structure, and as κ_l^p the line opacity that is purely photospheric.

3. Results and discussion

3.1. Chromospheric line blanketing

Figs. 2 and 3 show the ratio of κ_l^c to the total *continuous* mass absorption, κ_c, in the 500 to $12000A$ range for the lowest and highest pressure models in the $1A$ series, respectively. The dashed lines indicate the location of T_{min}. The value of $\frac{\kappa_l^c}{\kappa_c}$ reaches a local minimum near T_{min}, then begins to rise again with decreasing m in the lower chromosphere. This mirrors the rise of κ_l with increasing m in the upper photosphere just below T_{min}. In the upper chromosphere the higher temperatures dissociate molecules and ionize many metals leading to a decrease in κ_l^c in this wavelength regime, and finally an abrupt decline in the transition region. The initial rise in κ_l^c above T_{min} differs from the *ad hoc* gradual ramping down of κ_l above T_{min} in the cal-
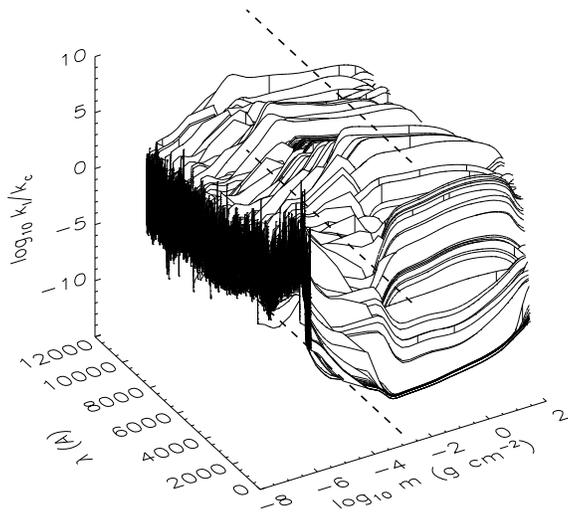
Fig. 2. Ratio of line to continuous absorption opacity, $\frac{\kappa_l^c}{\kappa_c}$, computed by PHOENIX for the lowest pressure model in $1A$ series. The dashed lines show the position of $T_{\min}$.
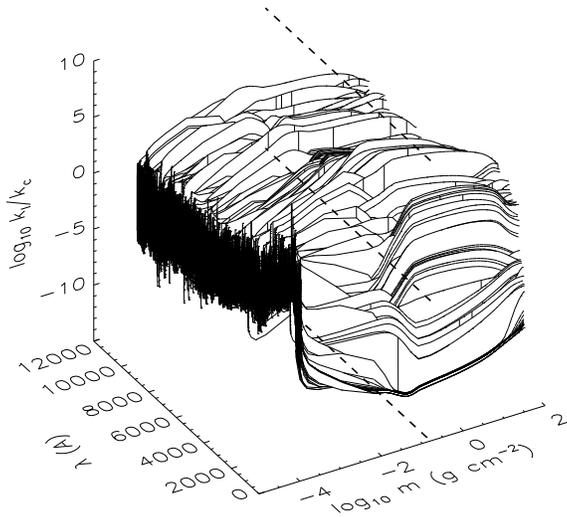

Fig. 3. Same as Fig. 2 for the highest pressure model in $1A$ series.

culations of ADB. Therefore, their treatment of transitions that form in the upper chromosphere and transition region are based on background opacities that are significantly under-estimated.

3.2. Radiative transfer in hydrogen

Fig. 4 shows the emergent flux, $F_\nu(\tau = 0)$, in the Lyman and Balmer continua as computed by MULTI for the lowest and highest pressure models in the $1A$ series, with κ_c only, with κ_l^p, and with κ_l^c. The Lyman jump is strongly in emission in the highest pressure model. The H I lines have been left out of κ_l because they are treated in detail in the MULTI calculation. All the important b-f continua of metals that are treated by the
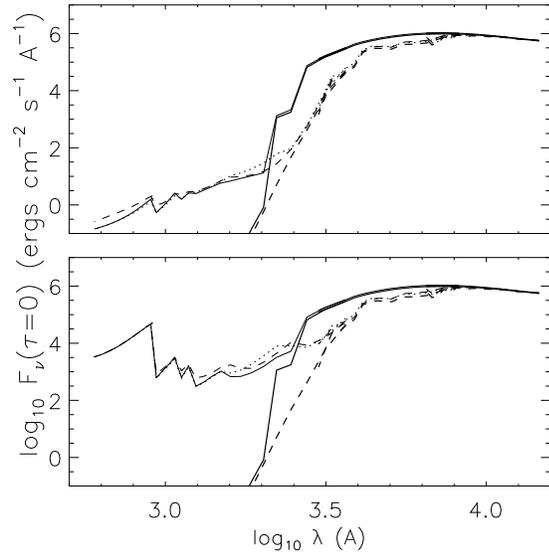

Fig. 4. The $F_\nu(\tau = 0)$ distribution for the radiative equilibrium model (thick lines), and chromospheric models of lowest (top panel) and highest (bottom panel) pressure in the $1A$ series. Solid line: κ_c only; dashed line: κ_l^c; dotted line: κ_l^p.

Uppsala Opacity package that accompanies MULTI have been included in all calculations. However, the presence of κ_l obscures the corresponding jumps in the $F_\nu(\tau = 0)$ distribution. In the region just to the blue of the Balmer jump, the inclusion of κ_l^c lowers $F_\nu(\tau = 0)$, which is consistent with the expected behavior of a blanketed radiation field. However, at still shorter wavelengths in the Balmer continuum, κ_l^c has the opposite effect and causes $F_\nu(\tau = 0)$ to be *larger*. For the lowest pressure model, this behavior extends to the blue side of the Lyman jump, where $F_\nu(\tau = 0)$ is larger by ≈ 0.5 dex in the case of κ_l^c. The main qualitative differences between the cases of κ_l^c and κ_l^p are that the κ_l^p predicts larger $F_\nu(\tau = 0)$ in the 1500 to $2500A$ range of the Balmer continuum, and lower $F_\nu(\tau = 0)$ in the Lyman continuum, compared to κ_l^c values.

Fig. 5 shows the mean intensity, J_ν, the monochromatic background intensity source function, S_ν, and the intensity contribution function, C_I, for an angle near disk center ($\mu = 0.887$), at two wavelengths on the Balmer continuum, for the cases of κ_c only, and κ_l^c values. The Planck function, B_ν, is also shown. For $\lambda \lesssim 3647A$, in both models, the inclusion of κ_l causes J_ν to be reduced throughout most of the atmosphere, as expected. However, the effect of κ_l^c on $F_\nu(\tau = 0)$ is controlled by the condition that $S_\nu \approx B_\nu$ at the depths where C_I is maximal, and the inclusion of κ_l^c causes the peak of C_I to move outwards. Because C_I peaks well below $T_{\min}$, the inclusion of κ_l^c causes $F_\nu(\tau = 0)$ to form at depths where B_ν is lower, and, hence, $F_\nu(\tau = 0)$ is reduced.

Further along the Balmer continuum, at $\lambda = 1600A$, the depth distribution of C_I is weighted more toward chromospheric depths, where $S_\nu \lesssim B_\nu$. The inclusion of κ_l^c raises the chro-
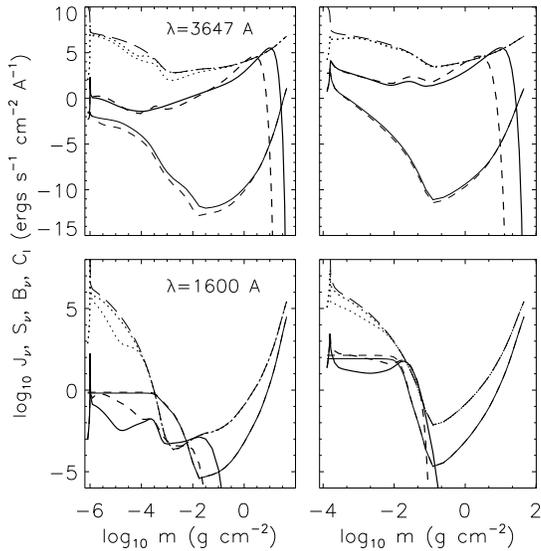
Fig. 5. Various radiative transfer quantities for $\lambda = 3647A$ (top panels) and $\lambda = 1600A$ (lower panels) for the lowest (left panels) and highest (right panels) pressure models in the $1A$ series. The thin solid line, thick solid line, and thin dotted line are J_ν, C_I, and S_ν, respectively, for $\mu = 0.887$, for the case of κ_c only. The thin short-dashed line, thick short-dashed line, and thick dotted line are the same quantities for the case of κ_1^c. The long-dashed line is B_ν.

mospheric part of C_I and shifts C_I to shallower depths above T_{min} where B_ν, and hence S_ν, is larger. Furthermore, the inclusion of κ_1^c raises S_ν in the upper chromosphere. Both of these effects cause $F_\nu(\tau = 0)$ to be increased. The increase in S_ν in the upper chromosphere in the case of κ_1^c is partly due to a very small *increase* in J_ν at these depths. Normally one expects line blanketing to decrease the value of J_ν. However, κ_1^c will generally include many lines that form at depths above T_{min}, and that have line source functions that are dominated by the thermal contribution ($S_1 \lesssim B_\nu$). At $\lambda < 3650A$ and $T \approx 6000$ K, B_ν is very sensitive to temperature, and at the chromospheric depths where these lines form, we may have the condition: $J_1 \approx B_\nu > J_{continuum}$. In other words, the chromospheric temperature inversion may drive many of these lines in to net emission, and κ_1^c may become a net contributor to J_ν in the UV. This is consistent with the greater size of the J_ν increase in the highest pressure model. The resulting increase in J_ν is slight and can only account for a small fraction of the increase in S_ν. The rest of the increase in S_ν in the case of line blanketing is the result of κ_1 being treated as a purely thermal source of opacity which, therefore, increases the relative contribution of B_ν to the value of S_ν.

Fig. 6 shows the same quantities as Fig. 5, but for $\lambda = 911A$. The situation differs from that of the Balmer continuum in that C_I is sharply peaked at depths in the uppermost chromosphere and transition region. Because of the much larger value of the continuous opacity in the Lyman continuum, $S_\nu = B_\nu$ throughout almost the entire atmosphere. However, in the lowest pressure model, $S_\nu \lesssim B_\nu$ in the uppermost part of the chromosphere
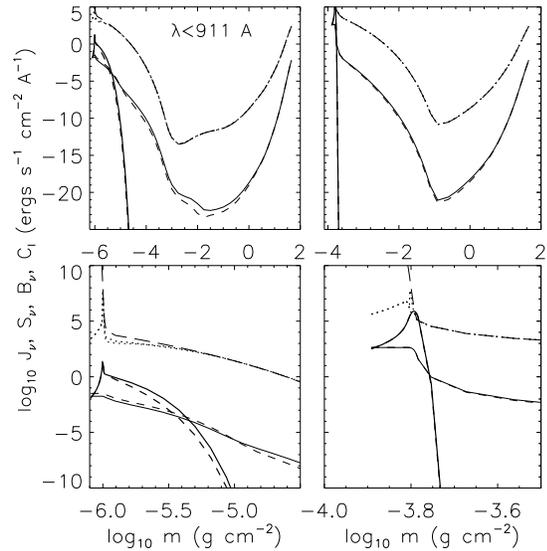
Fig. 6. Same as Fig. 5, but for $\lambda = 911A$. The lower panels show the same quantities as the upper panels, but on an expanded scale in column mass density.

where C_I is maximal. This slight departure from LTE allows the value of J_ν to influence S_ν, and furthermore, this figure shows that J_ν in the upper chromosphere is *increased* slightly by the inclusion of κ_1^c, as was the case at $\lambda = 1600A$. Therefore, S_ν, and consequently $F_\nu(\tau = 0)$, are increased by κ_1^c. For the highest pressure model, $S_\nu = B_\nu$ throughout the entire atmosphere, and C_I is so sharply peaked in the narrow transition region, that the inclusion of κ_1^c does not affect its location or value. Therefore, κ_1^c has negligible effect on $F_\nu(\tau = 0)$.

3.3. The N_{H_i} and N_e density structure

The left panel of Fig. 7 shows the radiative rate *per atom* from the $n = 1$ and $n = 2$ states of H I throughout the chromosphere in the same two models. Because the hydrostatic equilibrium population of H I and the statistical equilibrium population of the level populations may both be different for the cases with and without line blanketing, we show in the right panel the radiative rate per volume element. Figs. 5 and 6 show that for the lowest pressure model, in the case where κ_1^c is included, J_ν at 911 and $3647A$ is lower throughout the T_{min} region and most of the chromosphere. Correspondingly, the radiative ionization rates from $n = 1$ and $n = 2$ are lower throughout the chromosphere.

Fig. 8 shows the N_{H_I} and $N_{H_{II}}$ population densities normalized by the total H population density of the lowest and highest pressure models in the $1A$ series for the cases κ_c and κ_1^c. Fig. 9 show the corresponding N_e population density and also includes the case of κ_1^p. The effect of including κ_1^c is most pronounced in the lowest pressure model where it reduces N_e by as much as ≈ 0.3 dex at some depths in the chromosphere. The effect of κ_1^c is less pronounced in the highest pressure model. As expected, the decrease in N_e in the chromosphere caused
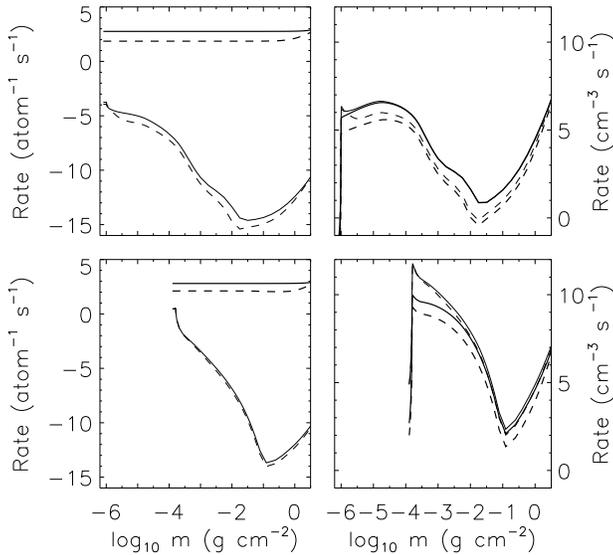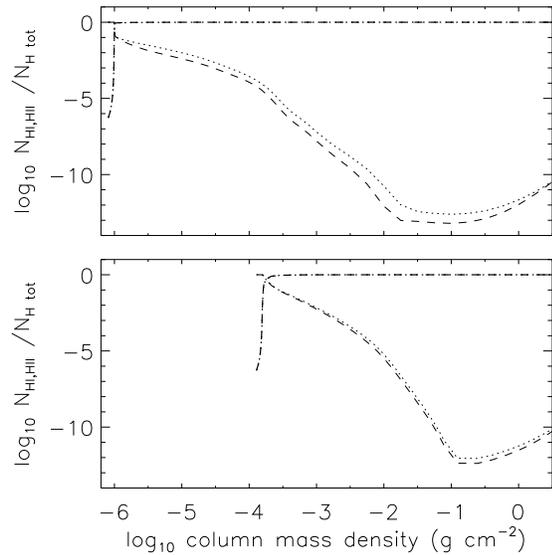
Fig. 7. Radiative ionization rates for H I from the $n = 1$ (thin lines) and $n = 2$ (thick lines) states for the lowest (top panel) and highest (bottom panel) pressure models in the $1A$ series. Solid line: κ_c only; dashed line: κ_1^c. Left panel: rates per atom; right panel: rates per unit volume.

Fig. 8. The $N_{\mathrm{H\,I}}/N_{\mathrm{H\,TOTAL}}$ (thick lines) and $N_{\mathrm{H\,II}}/N_{\mathrm{H\,TOTAL}}$ number density (thin lines) resulting from non-LTE H I solution for the lowest (top panel) and highest (bottom panel) pressure models in the $1A$ series. Dotted line: κ_c only; dashed line: κ_1^c.

by κ_1^c is mirrored by a corresponding decrease in $N_{\mathrm{H\,II}}$. However, the effect on the H I/H II balance due to κ_1^c persists deeper into the atmosphere by over two decades in column mass density than the effect on N_e. Unlike solar type stars, hydrogen remains mostly neutral until near the top of the chromosphere, as can be seen from Fig. 8. Therefore, the details of the H I/H II balance only have a significant effect on the N_e density in the upper chromosphere. As a corollary, we conclude that it is necessary to determine the effect of κ_1^c on the ionization equilibria of metals that are important electron donors in the lower chromosphere and $T_{\min}$ region, as well as on the H I/H II balance, in order to properly assess the sensitivity of the N_e density throughout the entire chromosphere to the opacity treatment.

The dotted line shows the N_e density resulting from a calculation with κ_1^p. The neglect of the chromospheric component of the line blanketing causes N_e to be underestimated by ≈ 0.05 dex near the top of the chromosphere in the lowest pressure model. In the highest pressure model, the two treatments of κ_1 produce N_e densities that differ negligibly.

Any differences in the final $N_{\mathrm{H\,I}}$ and N_e density that result from different treatments of the opacity may have two sources: 1) the H I/H II balance will differ as a result of different amounts of total opacity being included in the calculation of the radiative rates of the hydrogen transitions, 2) because the hydrostatic equilibrium equation was re-converged separately for each case, the equilibrium density structure differs for each case. In order to determine the relative importance of these two effects, we also show in Fig. 9 the N_e density normalized by the total H population ($N_e/(\mathrm{H\,I} + \mathrm{H\,II})$). Noting that the $y-$ axis scale is necessarily more compressed in the N_e/N_H plot, Fig. 9 shows that the differences in N_e between the cases with and without

κ_1^c are almost entirely due to direct radiative transfer effects on the H I/H II balance. The reduction in N_e and $N_{\mathrm{H\,II}}$ values due to κ_1^c are consistent with the reduction in radiative photo-ionization rate seen in Fig. 7 and this is consistent with the changes being directly due to radiative transfer effects. For the highest pressure model, the effect of κ_1^c on both the J_ν values and the radiative rates is rather smaller, which corresponds to the smaller effect on the N_e and $N_{\mathrm{H\,II}}$ densities.

3.4. The hydrogen spectrum

3.4.1. Lyα

Fig. 10 shows the Lyα flux profile for our entire grid with κ_c only and with κ_1^c. Also shown are line profiles for the $1A$ series with κ_1^p. The computed flux level of the emission peaks and the central reversal for all the models is negligibly affected by the inclusion of κ_1 and by the particular treatment of κ_1. Therefore, the absolute brightness of the line near $\Delta\lambda = 0$ may be used as an accurate chromospheric and transition region diagnostic without the inclusion of κ_1. However, the inclusion of κ_1^c causes the computed flux level of the continuum in the region of Lyα to be *increased* by as much as ≈ 0.3 dex. This increase is consistent with the behavior of the computed broad-band continuum shown in Fig. 4.

The increase in the local continuum level is reduced to the point of being negligible in the case of κ_1^p. The effect of including κ_1 in the photosphere, but neglecting it in the chromosphere, can be understood from a consideration of Figs. 5 and 6. For λ in the range 912 to 1600A, C_I arises largely at chromospheric depths. Therefore, κ_1^p neglects line blanketing in the part of the

Fig. 9. The N_e (left panel) and N_e/N_H (right panel) population density resulting from the non-LTE H I solution for the lowest (top panel) and highest (bottom panel) pressure models in the $1A$ series. Solid line: κ_c only; dashed line: κ_1^c, dotted line: κ_1^p.
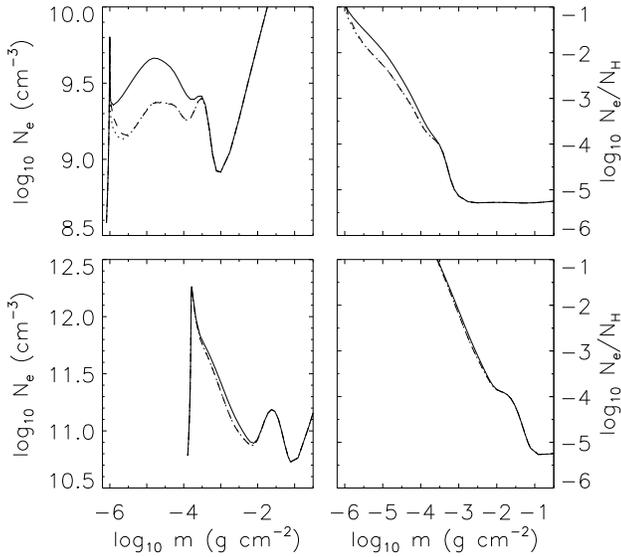
Table 2. W_λ of Lyα

| log m_0	W_λ in A		
$1A$ Series	κ_c	κ_1^p	κ_1^c
−6.0	−2.14e + 03	−2.04e + 03	−8.57e + 02
−4.8	−1.85e + 04	−1.86e + 04	−4.30e + 03
−3.8	−1.36e + 04	−1.50e + 04	−3.71e + 03

atmosphere where the background $F_\nu(\tau = 0)$ at $\lambda = 1215A$ is forming. Therefore, if the relative brightness of the line core with respect to the local continuum, or the equivalent width, W_λ, is to be used as a diagnostic, then the accuracy will be affected by the treatment of background opacity. Table 2 gives the W_λ values for the models of the $1A$ series with the various opacity treatments. The value of W_λ is reduced by as much as 75% by κ_1^c in the case of the highest pressure model. This large change in W_λ is difficult to see by visual inspection of Fig. 10. However, a ≈ 0.3 dex increase in the background $F_\nu(\tau = 0)$ corresponds to about a factor of five increase in linear flux units. Because the $F_\nu(\tau = 0)$ level of the line core does not change significantly when κ_1^c is added, the total area of the emission above continuum decreases by an amount that is approximately proportional to the increase in background $F_\nu(\tau = 0)$.

3.4.2. Hα

Fig. 11 shows the computed Hα profiles for the entire grid with κ_c only, and with κ_1^c. Also shown are line profiles for the $1A$ series only with κ_1^p. Table 3 shows the W_λ values for the models in the $1A$ series with the various opacity treatments. Compari-
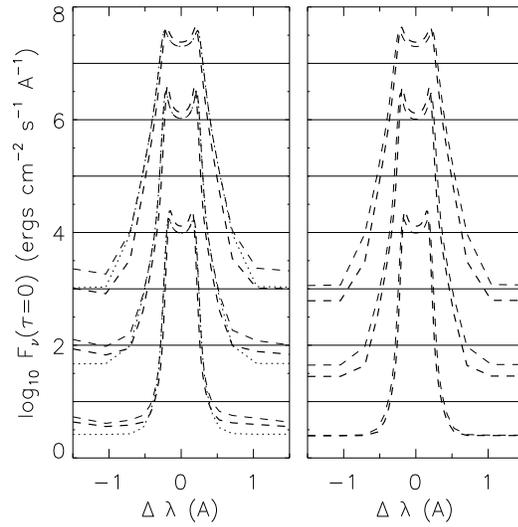
Fig. 10. Lyα flux profiles. Left panel: κ_1^c; right panel: κ_c only. Models in series $1A$: thin dashed line; $2A$ series: thick dashed line; the $1A$ series only with κ_1^p: dotted line. The lowest and highest pressure models are the ones that have the weakest and strongest line emission, respectively.
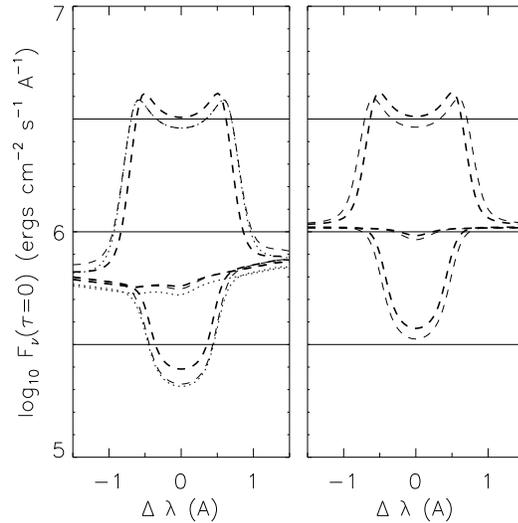
Fig. 11. Hα flux profiles. Left panel: κ_1^c; right panel: κ_c only. Models in series $1A$: thin dashed line; $2A$ series: thick dashed line; the $1A$ series with κ_1^p: dotted line. The lowest pressure models are the ones that have the weakest line absorption.

son of the left and right panels of Fig. 11 shows that inclusion of κ_1 causes the "continuum" to be noticeably depressed and distorted. It is not straight-forward to rectify the computed line profiles to a continuum level of unity because the background radiation is not a true continuum due to the inclusion of line blanketing. Therefore, we have plotted absolute flux and the comparison of line profiles between the calculations with and without κ_1 is with respect to their respective continua.

Historically, the morphology of Hα has been the main diagnostic for classifying dM stars by activity level, and Fig. 11

Table 3. W_λ of Hα

log m_0	W_λ in A		
1A Series	κ_c	κ_1^p	κ_1^c
−6.0	0.075	0.050	0.055
−4.8	0.710	0.680	0.705
−3.8	−3.560	−7.124	−6.375

Table 4. Integrated line flux in Lyα and Hα and Lyα/Hα in dMe (log $m_0 = -3.8$) models

Models	κ_c	κ_1^p	κ_1^c
	Lyα flux (ergs s^{-1} cm^{-2} A^{-1})		
1A Series	$1.57e+07$	$1.58e+07$	$1.57e+07$
2A Series	$1.64e+07$	$1.65e+07$	$1.65e+07$
	Hα flux (ergs s^{-1} cm^{-2} A^{-1})		
1A Series	$3.77e+06$	$4.41e+06$	$4.32e+06$
2A Series	$3.74e+06$	$4.34e+06$	$4.28e+06$
	Lyα/Hα		
1A Series	4.16	3.57	3.64
2A Series	4.40	3.81	3.87

shows that our grid spans the range of observed activity level from the least active dM(e) stars (profile with almost no absorption) to very active dMe stars (profile with the strongest emission). For the highest pressure model, the flux level of the emission peaks and central reversal are negligibly affected by κ_1^c, but the W_λ value of the net emission above continuum is approximately doubled due to the depression of the continuum. For the models where the profile is in absorption, the effect on W_λ is negligible. Therefore, Hα modelling of dMe stars in particular must incorporate κ_1^c in order to be accurate. The profiles of all the models are negligibly affected by the choice between κ_1^c and κ_1^p.

The Lyα to Hα flux ratio in dMe stars is a diagnostic of the thickness of the transition region (Houdebine & Doyle 1994). Table 4 shows the integrated line fluxes and the flux ratio in our most active models with the different treatments of line blanketing. The large dependence of W_λ on background opacity treatment shown in Tables 2 and 3 is proportional to a corresponding change in the background continuum level. Therefore, the total flux in the emission lines has a much weaker dependence. However, the Lyα to Hα flux ratio is reduced by ≈ 12 to 15% in the case of line blanketing. The flux ratio is only marginally affected by the choice between κ_1^p and κ_1^c. From Fig. 14 of Houdebine & Doyle (1994), we estimate that the neglect of line blanketing would cause an estimate of the transition region thickness based on a fit to Lyα/Hα flux to be too small by a factor of $\lesssim 2$. Doyle *et al.* (1997) present observed values of $F_{Ly\alpha}/H_{Ly\alpha}$ that have been corrected for the interstellar attenuation of Lyα for a variety of M drawfs. For Gl278C (dM1.0e), they find a value of 3.5, which is in excellent agreement with value calculated here with line blanketing included.
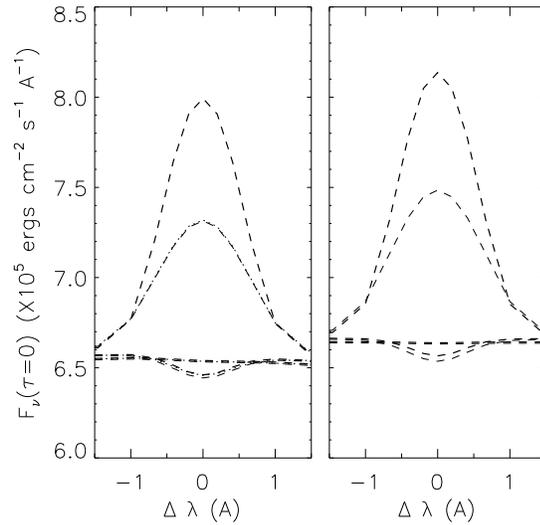
Fig. 12. Paβ flux profiles. Left panel: κ_1^c; right panel: κ_c only. Models in series 1A: thin dashed line; 2A series: thick dashed line; the 1A series with κ_1^p: dotted line. The lowest pressure models are the one with the weakest line absorption.

Table 5. W_λ of Paβ

log m_0	W_λ in mA		
1A Series	κ_c	κ_1^p	κ_1^c
−6.0	0.98	0.887	0.88
−4.8	18.22	16.00	17.88
−3.8	−178.49	−164.66	−163.91

3.4.3. Paβ

Recently, large gains have been made in detection technology in the near infrared spectral region. Therefore, the Paschen series of the H I spectrum has the potential to provide a useful diagnostic compliment to the Lyman and Balmer lines. Unfortunately, Paα ($\lambda18755$) lies in a region where telluric contamination is so large that the line is not a useful diagnostic. Therefore, we investigate the behavior of Paβ in our models. Fig. 12 shows the computed Paβ flux profiles with and without line blanketing. Also shown are line profiles for the 1A series with photospheric blanketing only. The lowest pressure models are the ones with almost non-existent absorption. Table 5 shows the W_λ values for the various cases. Fig. 12 shows that, for the highest pressure models, Paβ is much more sensitive to change in the chromospheric $\frac{dT}{d \log m}$ (or, equivalently, the location of T_{min}) than either Lyα or Hα. Therefore, this line provides a valuable additional constraint for semi-empirical models of dMe stars in particular.

The effect of background opacity treatment on the computed line profiles is marginal. The largest relative change is in the lowest pressure models where κ_1^c reduces W_λ by ≈ 10%. The decrease in sensitivity of the H I spectrum to the inclusion and

Table 6. Relative contribution to radiative cooling

	Unblanketed		Blanketed	
log m_0	Lines	Continuum	Lines	Continuum
Series 1A				
−6.0	0.000	0.000	0.000	0.000
−4.8	0.017	0.983	0.013	0.987
−3.8	0.174	0.826	0.114	0.886
Series 2A				
−6.0	0.001	0.999	0.006	0.994
−4.8	0.015	0.985	0.014	0.986
−3.8	0.190	0.810	0.164	0.836

treatment of κ_l as λ increases is consistent with the general decrease in spectral line blanketing as λ increases.

3.5. Chromospheric energy budget

One of the important conclusions of Houdebine *et al.* (1996) is that, contrary to what has been assumed previously, chromospheric radiative cooling in the emission continuum is greater than that in the H I emission lines for many chromospheric models. For their series of models with the largest value of T_{min} (3000K), they find that the relative contribution of the *total* H I series to the energy loss is at most 15%. For their lower T_{min} (2660K) models, the continuum contribution is about 50%. For both the lines and continuum, they define cooling as the excess flux above that from a basal flux model with minimal emission. The model with the lowest total emission (continuum + H I lines) in our grid is the lowest pressure model of the 1A series. We take this model as a fiducial basal flux star and subtract its H I line spectrum and continuum emission from each of the other models in the grid to produce excess emission values.

Table 6 shows the relative contribution to the total excess of the total H I line series up to and including the series of $n_l = 5$, and of the total H I continuum emission up to and including the B-F continuum of the $n = 5$ level. We confirm, qualitatively, the result of Houdebine *et al.* (1996) for the higher T_{min} models, where we find that the continuum carries over 80% of the excess flux at high chromospheric pressure. We also confirm the trend shown in their Fig. 7 toward increasing dominance of the continuum as chromospheric pressure decreases. However, our results differ radically from those of Houdebine *et al.* (1996) for lower T_{min} models, where we find that the continuum is dominant as in the higher T_{min} models. Lines play a minor role in the chromospheric energy loss throughout our entire grid. At this time we are unsure of the reason for the difference in the results for the lower T_{min} models. Fig 13 shows the overall distribution of $F_\nu(\tau = 0)$ for the entire grid. The strong response of the blue and UV continuum to increasing chromospheric pressure, combined with the large wavelength range over which the excess flux contributes, accounts for the dominant role of the continuum in the energy balance. Table 6 shows that the inclusion of κ_l^c has a minor effect on the relative contributions, and shifts the balance even more toward the continuum.
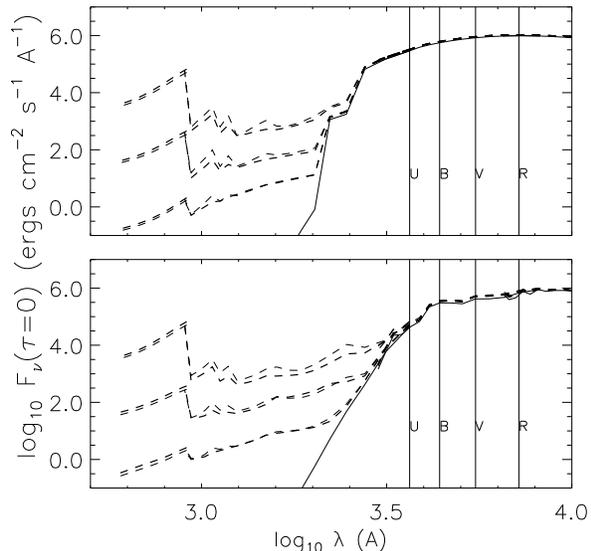
Fig. 13. Overall $F_\nu(\tau = 0)$ distribution for entire grid. Upper panel: κ_l^c; lower panel: κ_c only. Models in series 1A: thin dashed line; 2A series: thick dashed line; radiative equilibrium model: solid line.

These results are only approximate because the emergent flux in a transition is only equal to the total cooling in that transition if the transition is optically thin. The central double reversal of the Lyα and Hα line profiles indicate that there is some chromospheric self-absorption in these transitions and that, therefore, $\tau > 1$ at $\Delta\lambda \approx 0$. Therefore the cooling rate for a particular transition computed here and in Houdebine *et al* (1996), especially in the case of a line, is only a lower limit. Nevertheless, the dominance of the continuum in the total loss is so large that it is unlikely to be entirely due to an underestimate in the line cooling.

The amount of non-radiative heating required to energize the chromospheres of late-type stars is a fundamentally important constraint on theoretical heating mechanisms. Traditionally, the amount of heating has been measured by summing the excess flux in emission lines such as the H I Lyman and Balmer series and the Ca II and Mg II resonance doublets. However, the results shown here indicate that the energy loss in these lines may be only a small fraction of the excess flux in the continuum, and, therefore, the total cooling rates are much larger than previously thought.

3.6. Background non-LTE effects

3.6.1. Metallic $b - f$ continua

There are at least two important limitations in the computation of the emergent UV flux in both this work and in that of Houdebine *et al.* (1996). The first is that the background continuous absorbers have been treated in LTE. In their detailed modelling of the solar atmosphere, Vernazza *et al.* (1981) (VAL) showed that the continuum between 1000 and 1200 A is reduced by about an order of magnitude as a result, largely, of the ground

state C I $b - f$ continuum being out of LTE. VAL tabulate departure co-efficients, b_i, for the first eight levels of C I, Si I, Mg I, and Al I, and for eight combined levels of Fe I, all of which showed large non-LTE departures in their model. The lower excitation energy levels that are more heavily populated have b_i values that fall as low as ≈ 0.1 in the T_{min} region where the near UV continuum forms, and then rise to values of ≈ 100 in the upper chromosphere. To properly account for non-LTE metallic opacity in our models, we should solve the combined radiative transfer and statistical equilibrium equations for at least these five elements, then re-compute the non-LTE H I/II solution and hydrostatic equilibrium equation with the modified background opacity and metallic n_e contribution, and iterate this procedure until the n_e values converge at all depths. This is a massive computational undertaking and is beyond the scope of the current study. However, we intend to perform such a calculation once we have acquired all the necessary atomic data.

For now, we have made an initial estimate of the importance of metallic non-LTE departures with respect to the Sun in determining $F_\nu(0)$ in the UV by scaling the chromosphere and photosphere of the VAL solar model to one of our models (the lowest pressure model in the $1A$ series), and interpolating the VAL b_i values for the five metals listed above onto our model. We then recomputed $F_\nu(0)$ with the VAL b_i values incorporated into the calculation of the background opacity. There are at least two sources of error in this procedure: 1) The VAL b_i values are determined by the particular densities and radiative intensities in the VAL model; a full non-LTE treatment of the metals in our model will certainly yield different b_i values, and 2) we are only taking into account the non-LTE departures of the level populations; the $b - f$ source function, S_ν, is still equal to the Planck function in our calculation. Therefore, this is not a consistent non-LTE treatment of the background continuous opacity. Nevertheless, it gives us an approximate indication of the extent to which $F_\nu(0)$ is sensitive to the metallic b_i values as compared to the solar case.

The left panels in Fig. 14 show $F_\nu(0)$ with κ_c in LTE and with the VAL b_i values. The upper panel shows the important UV region and the lower panel shows the overall distribution. The left and right panels show the cases where κ_l blanketing is excluded and included, respectively. Careful examination of the upper panel shows that the 1000 to 1200 A region ($log\lambda = 3.0$ to 3.1 in the figure) is more affected by the metallic b_i values than the nearby regions, with the flux there being suppressed by non-LTE effects. This is in general agreement with the VAL results for the Sun, however, the effect is much less that the order of magnitude $F_\nu(0)$ reduction found for the VAL solar model. For both the VAL model and our dM star model, κ_c throughout most of the photosphere and lower chromosphere is dominated by C I around $\lambda 1000$ A and by C I and Si I around $\lambda 1200$ A, and in both cases the effect of non-LTE departures is to enhance the contribution of both metals so that they provide $\approx 100\%$ of the opacity. The difference in the behavior of $F_\nu(0)$ between the two models when departures are allowed for must depend on the exact location of the continuum formation in this region in each model. Due to the crudeness of our non-LTE treatment
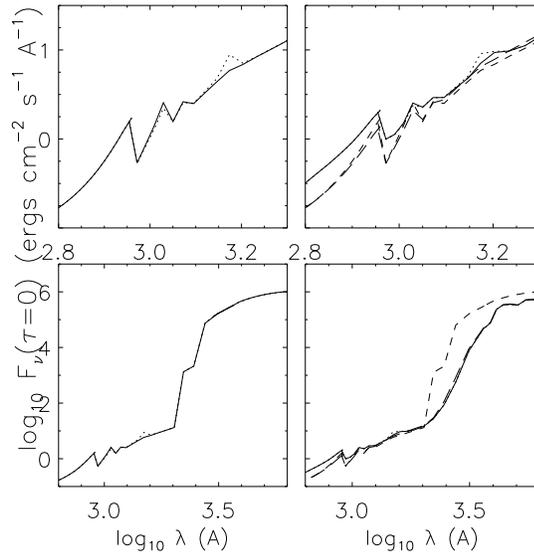
Fig. 14. The effect of various opacity treatments on $F_\nu(0)$. Left panels: κ_c only - LTE treatment (solid line), VAL b_i values for five metals (dotted line). Right panels: κ_l^c blanketing - κ_c in LTE (solid line), κ_c with VAL b_i values (dotted line), κ_c in LTE and a line scattering albedo in κ_l for the case of minimal scattering (long dashed line) and Anderson's atomic scattering (short dashed line). Top panels: UV region. Bottom panels: overall distribution.

in the M star model, further analysis of the difference in $F_\nu(0)$ behavior between the two models is unwarranted at this time. Inspection of the right panel shows that the $F_\nu(0)$ suppression due to non-LTE $b - f$ effects is reduced to negligibility by the inclusion of line opacity.

Also, we find an enhancement in $F_\nu(0)$ due to non-LTE departures in the $log\lambda = 3.15$ to 3.2 region. At $\lambda = 1500A$ the dominant contributor changes from Si I to a combination of Si I, Mg I, and Al I as λ increases. These metals contribute close to 100% of the opacity in both the LTE and non-LTE case. Once again, an explanation of the excess $F_\nu(0)$ in the non-LTE case will require a careful study of where the continuum forms and should wait until the non-LTE treatment of metals in our model is treated properly.

We conclude tentatively that the impact of metallic non-LTE departures on the UV emission in our models is significantly less that found for the Sun by VAL and probably does not effect our conclusion that the continuum emission dominates the chromospheric energy budget. However, a self-consistent solution of the non-LTE problem for hydrogen and all five dominant metals must be undertaken for our models before we can reach a definite conclusion on this point.

3.6.2. Background line scattering

The second limitation in this work is that the line blanketing opacity, κ_l, is assumed to be entirely thermal throughout the model. The extensive non-LTE line blanketing calculation of Anderson (1989) for the Sun demonstrates that many atomic
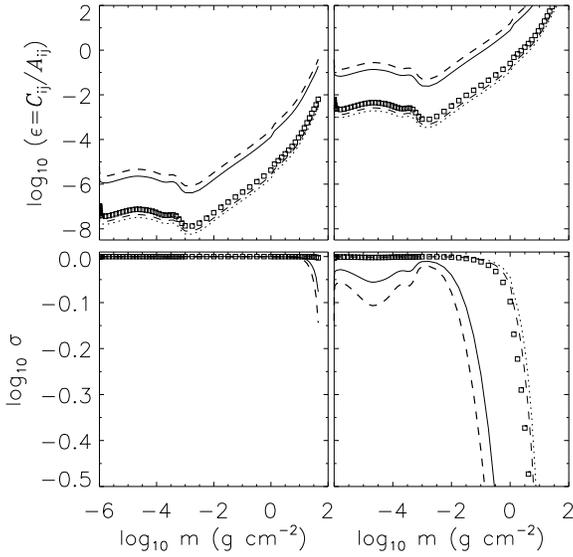
Fig. 15. Top panel: approximate line thermalization parameter, ϵ at 926 A (dotted line), 1026 A (dashed line), 1226 A (squares), 3836 A (solid line), 4863 A (thick dashed line). Bottom panels: line scattering albedo, σ. Anderson's albedo parameter, q, equal to 6.0×10^{12} (left panels), and 1.0×10^9 (right panels).

and ionic lines become scatterers rather than thermal absorbers of radiation in the upper photosphere of a radiative equilibrium model where the gas density becomes relatively low. As a result, our thermal treatment has the effect of keeping S_ν artificially close in value to B_ν in the outer layers where the UV continuum is forming. In the case of coherent isotropic scattering the line source function, S_1, is approximately given by

$$S = \frac{J + \epsilon B}{1 + \epsilon}, \tag{1}$$

and the extent to which a line is scattering rather than absorbing is determined by the relative weights of J and B in this sum. The line thermalization parameter, ϵ, is equal to C_{ij}/A_{ij}, where C_{ij} is the rate of collisional transitions between the upper and lower states, and A_{ij} is the rate of spontaneous radiative decay from the upper state. The dependence on C_{ij} makes ϵ depth dependent, and Anderson (1989) has suggested the following approximate formula for ϵ:

$$\epsilon = \frac{N_e}{q(h\nu)^3}, \tag{2}$$

where $h\nu$ is in eV and $q = 6 \times 10^{12}$ for Fe I lines and 7×10^{13} for ionic lines. Furthermore, the line scattering albedo, σ, is equal to $1/(1 + \epsilon)$.

We have modified our treatment of κ_1 by adding the quantity $\sigma \times \kappa_1$ to the total scattering opacity and $(1 - \sigma) \times \kappa_1$ to the total thermal opacity at each depth. The purely thermal treatment of κ_1 that was described in the previous sections corresponds to the case of $\sigma = 0$. Our κ_1 tables include all lines from atoms, ions, and molecules added together. Therefore, we are not able to treat lines from different types of absorbers separately. However, we have tried two extreme values of q found in the literature:

Table 7. Relative flux excess in UBV with respect to basal model (series $1A$, $\log m_0 = -6.0$)

log m_O	Unblanketed			Blanketed		
	U	B	V	U	B	V
Series $1A$						
-6.0	0.000	0.000	0.000	0.000	0.000	0.000
-4.8	0.012	0.010	0.008	0.030	0.023	0.026
-3.8	0.039	0.023	0.018	0.151	0.049	0.078
Series $2A$						
-6.0	0.007	0.005	0.004	0.030	0.008	-0.002
-4.8	0.017	0.014	0.011	0.027	0.023	0.025
-3.8	0.038	0.022	0.017	0.275	0.091	0.043

Anderson's atomic value of 6×10^{12}, and a value of 1.0×10^9 that that corresponds to mostly thermal lines with minimal scattering (Avrett *et al.* 1994). The right panels of Fig. 14 show the computed $F_\nu(0)$ with σ included in the treatment of κ_1. Fig. 15 shows the value of ϵ and σ throughout the model for both values of q.

For $q = 6 \times 10^{12}$, ϵ, as computed by the approximate formula, is very low ($< 10^{-4}$) throughout most of the model above the deep photosphere. As a result, σ is almost unity and $F_\nu(0)$ for $\log\lambda > 3.3$ is an order of magnitude brighter than that of the thermal case and is indistinguishable from that of an unblanketed model because the lines are barely absorbent. However, for $\log\lambda < 3.3$, $F_\nu(0)$ is reduced by ≈ 0.2 dex with respect to the thermal case. Höflich (1995) has suggested that the value of ϵ based on the treatment of Anderson (1989) may be as much as two orders of magnitude too small, which may account for the underblanketing found with the atomic q parameter at $\log\lambda > 3.3$. At the other extreme, $q = 1 \times 10^9$ gives an $F_\nu(0)$ distribution that differs negligibly from the purely thermal $F_\nu(0)$ for $\log\lambda > 3.3$. For $\log\lambda < 3.3$, $F_\nu(0)$, is very close to that computed with the much higher q value. This relative insensitivity of the mid-UV flux to the albedo is due to the rapid increase of σ with decreasing N_e and decreasing λ, which causes σ to be ≈ 1 at the depths where radiation with $\lambda < 3.3$ forms for both values of q.

The 0.2 dex decrease in the UV flux due to line scattering with either extremal value of q is much less than the four orders of magnitude difference between the UV $F_\nu(0)$ values for the chromospheric model and the radiative equilibrium model. We conclude, for now, that the chromosphere produces substantial excess continuum emission, even in the presence of blanketing by scattering lines.

The extent to which the non-LTE departures discussed above affect $F_\nu(0)$ may depend on the chromospheric pressure. Therefore, these effects will be investigated, more accurately, for the entire grid of models in a future study.

3.7. Photometric colours

Houdebine *et al.* (1996) have found that in the highest pressure chromospheric models, the structure of the outer atmosphere has

Table 8. Computed colours of grid models

	Unblanketed		Blanketed	
$\log m_0$ TR	$U - B$	$B - V$	$U - B$	$B - V$
Series $1A$				
-6.0	0.286	1.031	1.481	1.123
-4.8	0.284	1.029	1.473	1.126
-3.8	0.269	1.027	1.381	1.151
Series $2A$				
-6.0	0.285	1.030	1.458	1.111
-4.8	0.283	1.028	1.477	1.124
-3.8	0.270	1.026	1.312	1.073

a detectable effect on the $U - B$ colour due to the increasing enhancement of $F_\nu(\tau = 0)$ with decreasing λ seen in Fig. 13. In Table 7, we show for our grid of models with and without line blanketing the excess flux with respect to the basal model normalized by the flux from the basal model in the Johnson UBV pass-bands. In Table 8, we show the computed $U - B$ and $B - V$ colours. For the unblanketed models, the highest pressure model has a value of $U - B$ that is 0.015 magnitudes lower than that of the lowest pressure model. The changes in $F_\nu(\tau = 0)$ due to the addition of κ_1^c increase $U - B$ by ≈ 1.1 magnitudes and $B - V$ by ≈ 0.3 magnitudes. The sensitivity of $U - B$ to chromospheric pressure is reduced somewhat in the presence of κ_1, but is still significant; the difference between the lowest and highest pressure models is reduced to ≈ 0.01 magnitudes. Therefore, we confirm the result of Houdebine *et al.* (1996) that the chromospheres of the most active stars should be detectable with centimagnitude precision broad band photometry in the violet and blue spectral regions.

Amado & Byrne (1997) have analysed de-reddened two-colour diagrams in the Johnson system for a large sample ($n > 100$) of late-type stars with $B - V$ in the range 0.2 to 2.2. They have found that stars classified as "active" on the basis of their observed Hα profile, on average, have a $U - B$ colour that is 0.042 magnitudes bluer, with $\sigma = 0.0872$, than inactive stars. They caution that the dependence of colour on metallicity has not been accounted for in their study. However, their results suggest that there is a $U - B$ dependence on chromospheric activity at the centimagnitude level found in our calculations.

4. Conclusion

The predicted W_λ of the Lyα emission line is strongly reduced, and that of the Hα emission line in active (dMe) stars is strongly enhanced by the inclusion of line blanketing in the background opacity in the non-LTE hydrogen calculation. In less active stars only Lyα is significantly affected. Furthermore, to calculate W_λ for Lyα accurately, the calculation of κ_1 must be *consistent* in that it must reflect the chromospheric and transition region temperature rise. The calculated Paβ line is negligibly affected by the inclusion, and particular treatment, of κ_1. We conclude that a careful teatment of background opacity is important when using

Hα to model relatively active dM stars and flares, or when using Lyα emission *relative to the local continuum* as a diagnostic.

The inclusion of κ_1^c *raises* $F_\nu(\tau = 0)$ in the Lyman continuum in the lowest pressure models, and *raises* $F_\nu(\tau = 0)$ in the Balmer continuum for $\lambda < 2500A$ in the highest pressure models, by a factor of ≈ 3. In both cases, line blanketing directly causes a slight rise in J_ν in the region where C_I is maximal. This, combined with a partial decoupling of S_ν from B_ν, leads to the increase in $F_\nu(\tau = 0)$. This suggests that, in these spectral regions, κ_1^c is a net source of emission and contributes positively to $F_\nu(\tau = 0)$. Furthermore, the thermal treatment of κ_1 strengthens the coupling of S_ν to B_ν in the upper chromosphere where B_ν is increasing rapidly and this also causes the value of S_ν to be larger in the case of line blanketing.

We confirm two of the most important results of Houdebine *et al.* (1996): the photometrically detectable influence of the highest pressure chromospheres on the U band flux, and the dominance of the continuum in the radiative cooling of the chromosphere. We disagree with the results of Houdebine *et al.* (1996) in detail in that we find that the continuum dominates the cooling for all models with T_{min} in the 2600 to 3000 K range, whereas they find that the continuum dominates only in the case of models at the hot end of the range. In either case, this result has important implications for the general problem of chromospheric heating because it greatly changes the estimated energy budget of the outer atmosphere. If this result is correct, and comparison with the observational analysis of Amado & Byrne (1997) suggest that it is, then proposed heating mechanisms must supply at least an order of magnitude more non-radiative heating to the chromosphere than would be needed in the case of an energy analysis based only on lines.

An important caveat to these conclusions is that the emergent UV flux in late type stars in known to be sensitive to non-LTE effects in the background opacity of both lines and continua. We have estimated the size of the expected effect in both cases for one of the models in our grid, crudely for the case of $b - f$ continua. These non-LTE effects must be calculated more accurately for the entire grid of models before the role of continuum emission in the chromospheric energy budget can be assessed precisely.

References

Amado, P. & Byrne, P. B., 1997, A&A, *in press*
Allard, F., & Hauschildt, P. H., 1995, ApJ, 445, 433
Anderson, L. S., 1989, ApJ, 339, 558
Andretta, V., Doyle, J. G., & Byrne, P. B., 1997, A&A, *in press*

Avrett, E. H., 1990, in IAU Symposium 138, Solar Photosphere: Structure, Convection, and Magnetic Fields., ed. J. O. Stenflo (Dordrecht: Kluwer), p. 3

Avrett, E. H., Chang, E. S., & Loeser, R., 1994, in IAU Symposium 154, Infrared Solar Physics, eds. D. M. Rabin, J. T. Jefferies, and C. L. Lindsey (Dordrecht: Kluwer), p. 323

Basri, G. S., Linsky, J. L., & Eriksson, K., 1981, ApJ, 251, 162

Carlsson, M., 1986, Uppsala Observatory Internal Report no. 33

Doyle, J. G., Houdebine, E. R., Mathioudakis, M., & Panagi, P. M., 1994, A&A, 285, 233

Doyle, J. G., Mathioudakis, M., Andretta, V., Short, C. I., & Jelinsky, P., 1997, A&A, *in press*

Drake, J. J., 1991, MNRAS, 251, 369

Eriksson, K., Linsky, J. L., & Simon, T., 1983, ApJ, 272, 665

Haisch, B., Strong, K. T., & Rodono, M., 1991, ARA&A, 29, 275

Höflich, P., 1995, ApJ, 443, 89

Houdebine, E. R. & Doyle, J. G., 1994, A&A, 289, 169

Houdebine, E. R., Doyle, J. G., & Koscielecki, M., 1995, A&A, 294, 773

Houdebine, E. R., Mathioudakis, M., Doyle, J. G., & Foing, B. H., 1996, A&A, 305, 209

Kelch, W. L., Linsky, J. L., & Worden, W. P., 1979, ApJ, 229, 700

Kurucz, R. L., 1990, Transactions of the IAU, XXB, ed. M. McNally (Dordrecht: Kluwer), p. 168

Lang, K. R., 1992, Astrophysical Data: Planets and Stars, (Springer-Verlag: New York)

Luttermoser, D. G., Johnson, H. R., & Eaton, J., 1994, ApJ 422, 351

Mauas, P. J. D. & Falchi, A., 1996, A&A 310, 245

Mihalas, D., 1978, Stellar Atmospheres, 2nd ed., (W. H. Freeman and Co.)

Mihalas, D. & Binney, J., 1981, Galactic Astronomy, 2nd ed., (W. H. Freeman and Co.)

Rutten, R. J., 1988, in IAU Coll. 94, Physics of formation of FeII lines outside LTE, R. Viotti, A. Vittone, and M. Friedjung, eds. (Dordrecht: Reidel), p. 185

Vernazza, J. E., Avrett, E. H., & Loeser, R., 1981, ApJS, 41, 635